Supplemental Materials

Molecular Biology of the Cell

Dymek et al.

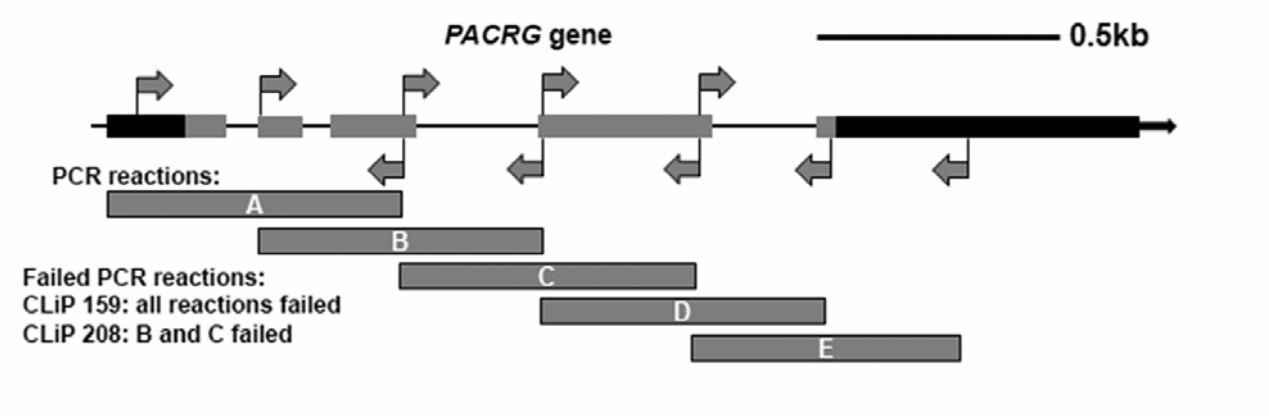

Supplemental Figure 1. Diagram of the amplified products across the *PACRG* gene to test for the CLiP insertion. Five overlapping pieces of the *PACRG* gene were amplified from wild-type or CLiP mutant (159 and 208) genomic DNA. A fragment of C1a-86 genomic DNA was amplified from wild-type, 159 and 208 genomic DNA as a control. All of the above reactions were amplified successfully from wild-type genomic DNA. None of the above reactions were able to be amplified from 159 DNA, indicating an entire gene knockout. Reactions B and C failed to amplify from 208 DNA, indicating an insertion site between exons 3 and 4.

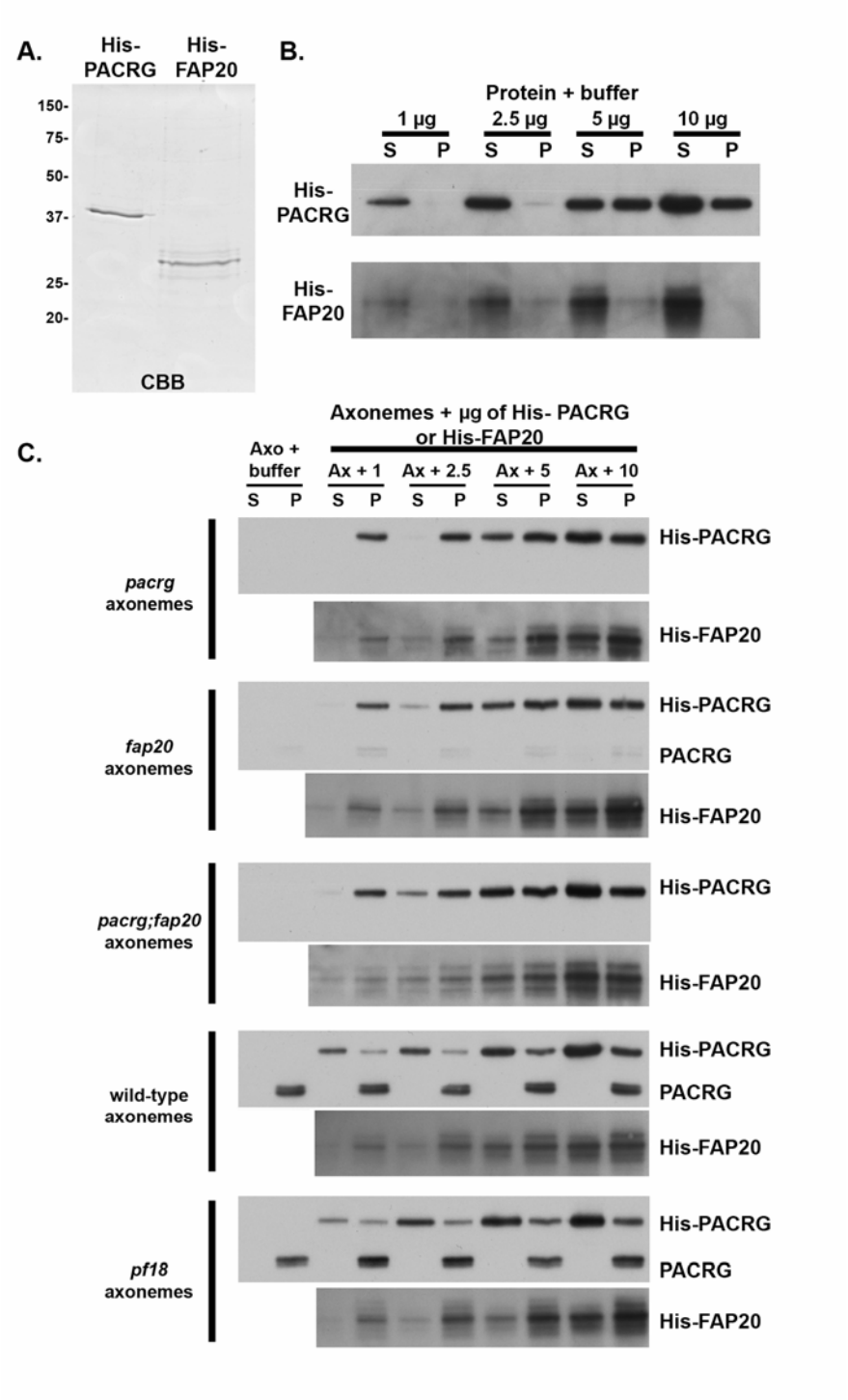
A.
His-PACRG
His-FAP20
150-
75-
50-
37-
25-
20-
CBB
B.
Protein + buffer
1 µg
2.5 µg
5 µg
10 µg
S P S P S P S P
His-PACRG
His-FAP20
C.
Axonemes + µg of His- PACRG or His-FAP20
Axo + buffer
Ax + 1
Ax + 2.5
Ax + 5
Ax + 10
S P S P S P S P S P
pacrg axonemes
His-PACRG
His-FAP20
fap20 axonemes
His-PACRG
PACRG
His-FAP20
pacrg;fap20 axonemes
His-PACRG
His-FAP20
wild-type axonemes
His-PACRG
PACRG
His-FAP20
pf18 axonemes
His-PACRG
PACRG
His-FAP20

Supplemental Figure 2. Purified His-PACRG and His-FAP20 can specifically and efficiently bind to isolated mutant axonemes. (A) Coomassie brilliant blue stained gel of bacterially expressed and purified His-PACRG and His-FAP20 (1 µg of protein loaded for each). (B) Anti-PACRG and S-tag-HRP blots of His-PACRG and His-FAP20, respectively. As a control for (C), various amounts of purified protein were mixed with buffer (klow), incubated at RT for 15' and centrifuged at 10,000 X g for 10'. Supernatant (S) were transferred to a new tube and pellets (P) were resuspended in an equal volume. The majority of His-PACRG or His-FAP20 is found in the supernatant, until 5 µg or more is added. (C) Binding of His-PACRG and His-FAP20 to 25 µg of axonemes. For His-PACRG, binding saturation occurs at 2.5 µg of purified protein and 25 µg of *pf12* axonemes. Small amounts of His-PACRG pellet with WT or *pf18* axonemes, even though endogenous PACRG protein is present. His-FAP20 saturates binding to *fap20* axonemes near 2.5 µg per 25 µg of axonemes. His-FAP20 also pellets with WT and *pf18* axonemes. It is not clear if this represents nonspecific binding, however, this apparent non-specific binding has no affect on sliding velocity of *pf18* axonemes (see Fig 3). Blots were probed with anti-PACRG to detect His-PACRG and endogenous PACRG or S-tag-HRP to detect His-FAP20.

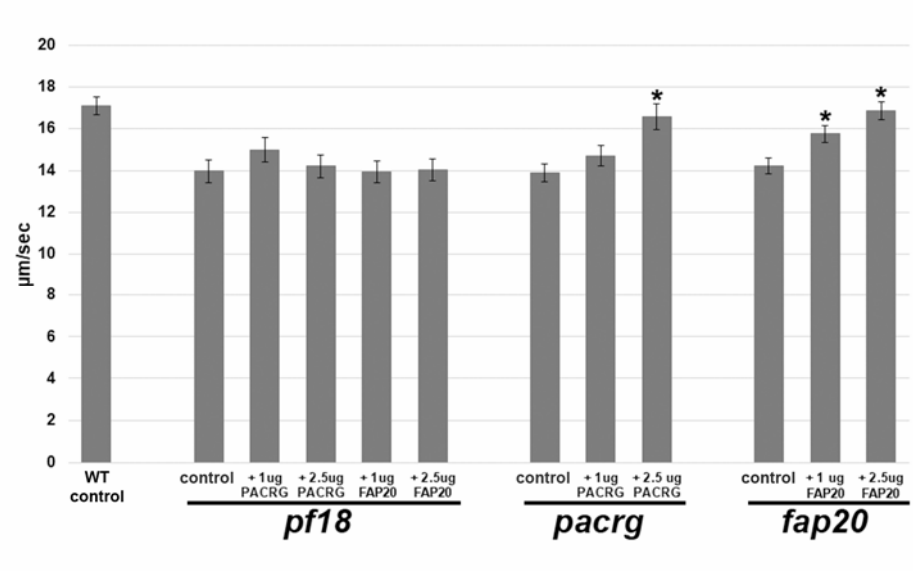

Supplemental Figure 3. Microtubule sliding velocities with purified PACRG or FAP20 added to axonemes in a dose-dependent manner. Both *pacrg* (*pf12*) and *fap20* (RL11) mutant microtubules have a slower sliding velocity than wild-type in sliding buffer. Once their respective purified protein is added to the isolated axonemes (His-PACRG or His-FAP20), velocities increase in a dose-dependent manner. As a control, *pf18* axonemes show no increase in microtubule sliding velocity with either purified protein in either amount. Asterisk = value is significantly different than the same strain's value in sliding buffer.

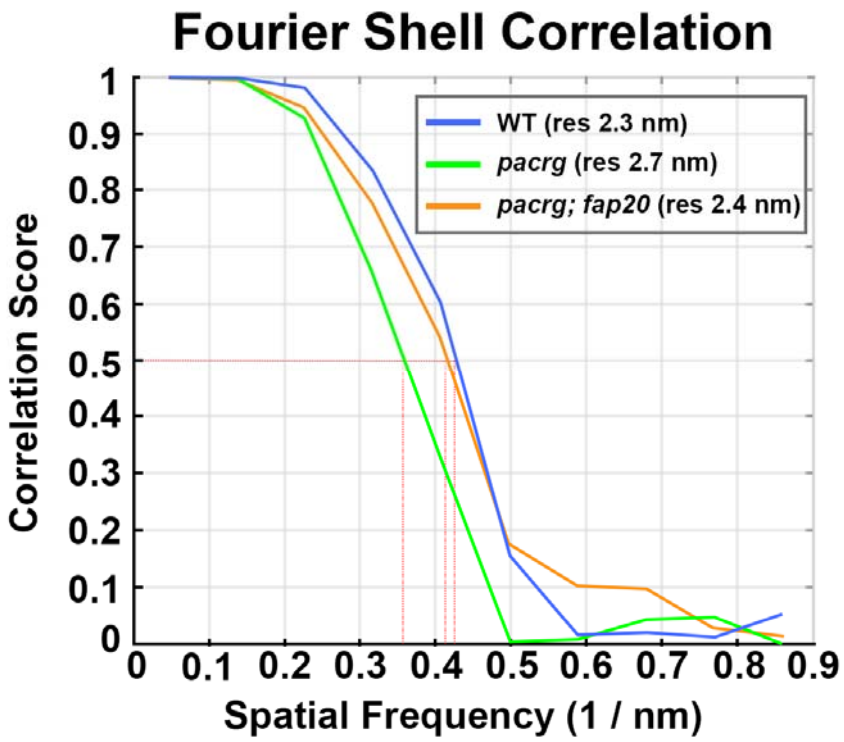

Supplemental Figure 4. Fourier shell correlation plots show the resolution (0.5 criterion) for the subtomogram averages of wild type (blue), *pacrg* (green), and *pacrg; fap20* (orange) axonemes.

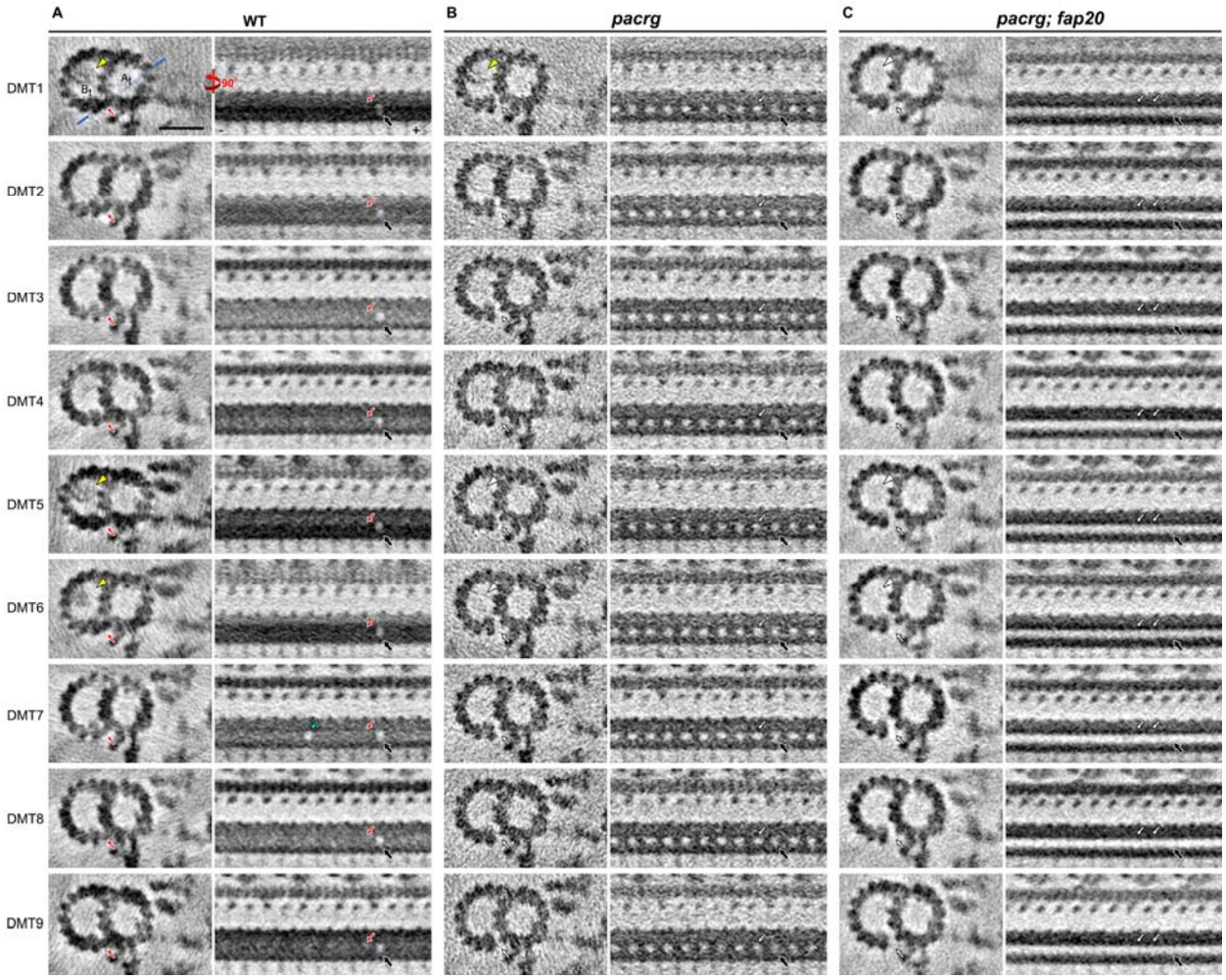

Supplemental Figure 5. Doublet-specific averaging shows that the inner junction defects are visible in all nine doublet microtubules of *pacrg* and *pacrg; fap20* axonemes. Tomographic slices show cross-sections (left; 3 nm-thick) and longitudinal sections (right; 2 nm-thick) of the averaged 96-nm axonemal repeats from the 9 individual outer doublet microtubules (DMTs 1-9) of *Chlamydomonas* WT (A), *pacrg* mutant (B) and *pacrg; fap20* double mutant (C) axonemes. The location of the longitudinal tomographic slices is indicated by a blue line in (A) (DMT1, left). The densities that were present in wild-type axonemes but missing from the mutants are highlighted by red and white arrows, respectively. Note that an additional, previously undescribed IJ hole (black arrows) was discovered on DMT7 in wild-type (blue arrow). Note also that the beak-MIP structures were detected in DMTs 1, 5, and 6 of wild-type axonemes, but only a weak density was observed in *pacrg* DMT1. Microtubule polarity (+ and - end). Scale bar: 20 nm (A, valid for all panels).

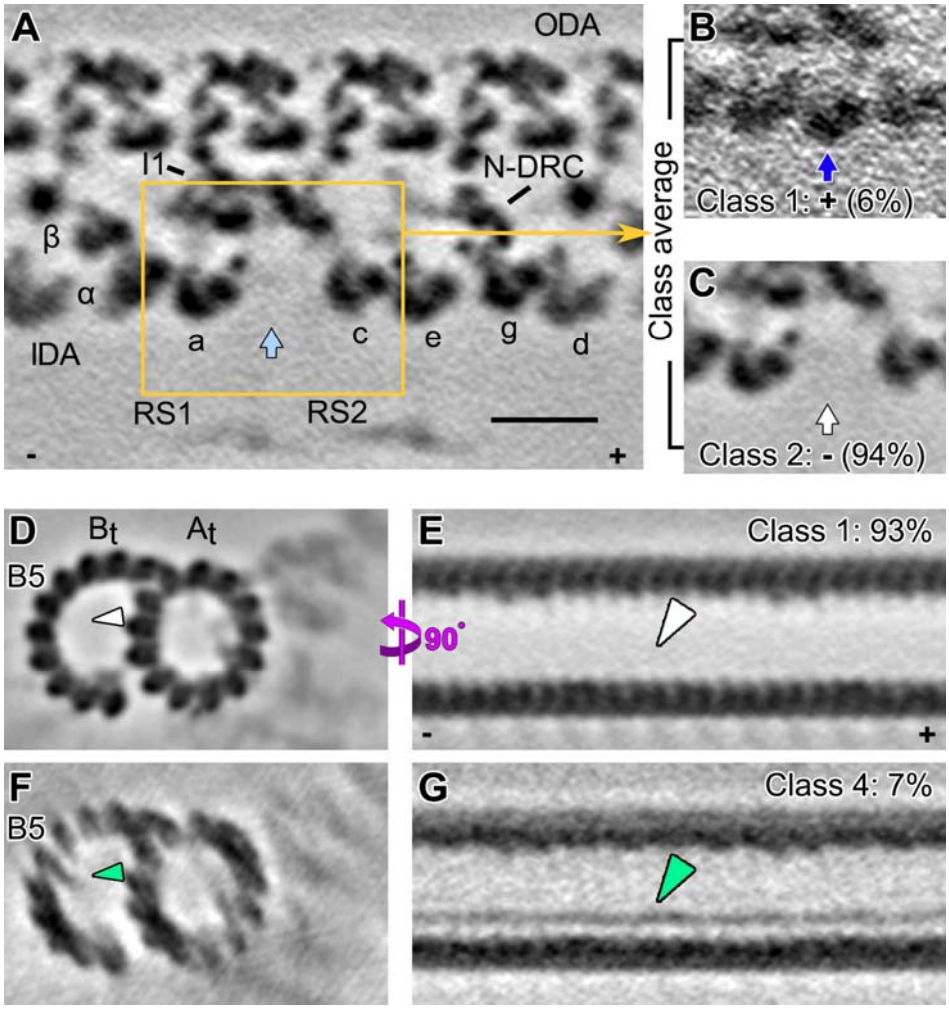

Supplemental Figure 6. Classification analyses identified structural defects of the inner dynein arm IDA b and the beak-MIP in *Chlamydomonas pacrg; fap20* double mutant. (A-C) Classification analyses of IDA b. Longitudinal tomographic slice (5 nm thick) of the average of all axonemal repeats (A) show the significantly reduced IDA b (light blue arrow), which was classified into two classes: with (blue arrow in B, Class 1) and without IDA b (white arrow in C, Class 2). The percentage of each class average is indicated. (D-G) Classification analyses of the beak-MIP in the B-tubule. Cross-sectional (D and F, 50 nm thick) and longitudinal (E and G, 5 nm thick) tomographic slices of the class-averaged axonemal repeats show only 2 classes: missing the beak-MIP structure (white arrowheads in D and E, Class 1) and a reduced beak-MIP with only one ribbon extending from protofilament B5 (green arrowheads in F and G, Class 4). The class names were assigned based on the classification results of *pacrg* mutant in Figure 6 and the percentage of each class average is indicated. Other labels: A-tubule (At), B-tubule (Bt), nexin-dynein regulatory complex (N-DRC), radial spoke (RS), outer dynein arms (ODA), microtubule polarity (+ and - end). Scale bar: 20 nm (A, valid for all panels).

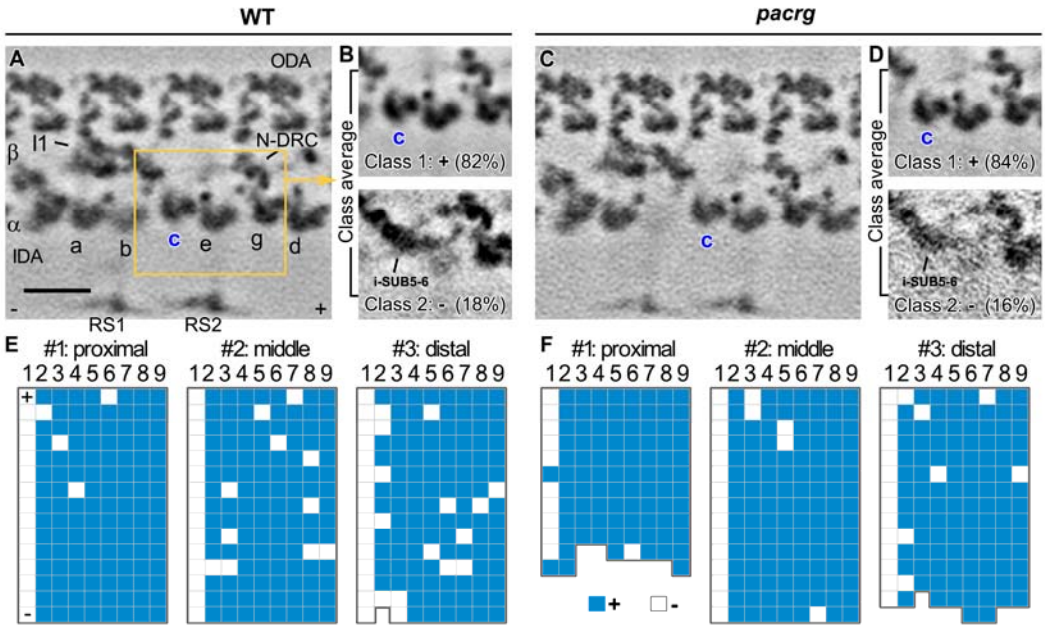

Supplemental Figure 7. As control, the classification analyses of inner arm dynein IDA c showed no structural differences between wild-type and *pacrg* mutant axonemes. (A-D) Longitudinal tomographic slices of the averaged axonemal repeats show comparable densities of IDA c (blue) in wild-type (A and B) and *pacrg* mutant axonemes (C and D), both in all repeat averages (A, C) and in class averages (B, D); the percentage of each class average is indicated. Note that the classification identified the previously described i-SUB5-6 structure between Chlamydomonas DMT1 and DMT2 (Lin *et al.*, 2012). (E and F) Distributions of axonemal repeats with (blue grids) and without IDA c (white grids) in three different regions of individual flagella of wild-type (E) and *pacrg* mutant strain (F). In the distribution patterns, the repeats on the nine DMTs (1-9) are schematically shown as individual grids. Microtubule polarity (+ and - end). Scale bar: (A-D) 20 nm.

Supplemental Video 1. Video of a wild-type cell swimming forward with an asymmetric waveform. Cells were captured at 500 fps using a pco.1200HS camera and videos created at 30 fps with Camware (The Cooke Corporation, Londonderry, NH) and ImageJ (Schneider *et al.*, 2012) software.

Supplemental Video 2. Video of a *pacrg* mutant cell (CLiP 159) with abnormal waveform and motility. Cells were captured at 500 fps using a pco.1200HS camera and videos created at 30 fps with Camware (The Cooke Corporation, Londonderry, NH) and ImageJ (Schneider *et al.*, 2012) software.

Supplemental Video 3. Video of a *pacrg* mutant cell (*pf12*-cc1031) with abnormal waveform and motility. Cells were captured at 500 fps using a pco.1200HS camera and videos created at 30 fps with Camware (The Cooke Corporation, Londonderry, NH) and ImageJ (Schneider *et al.*, 2012) software.

Supplemental Table 1. Primer sequences used to amplify CLiP 159 and 208 genomic DNA to identity an insertion site.

Primer pairs	Size of amplified product
F1 5' CGTTAATCACTCGCTTACAGTTCG 3' R1 5' GCAAGTCGCCACGCTCGTAGAAGC 3'	693 bp
F2 5' GCTTTGACACGACATCGCTATCG 3' R2 5' GCAGGTAGTGGTGGTAGTCCAGC 3'	735 bp
F3 5' GCTTCTACGAGCGTGGCGACTTGC3' R3 5' CCATAGTCAATGCCGTCGCCC 3'	694 bp
F4 5' GCTGGACTACCACCACTACCTGC 3' R4 5' GCGTAGTTCACGCTGGACTCG 3'	732 bp
F5 5' GGGCGACGGCATTGACTATGGC 3' R5 5' GCGAACGATGCATCGTCAAGACC 3'	677 bp

Supplemental Table 2. Primer sequences used to amplify *pf12* DNA for sequencing.

Primer pairs	Size of amplified product
F1 5'-AGCGGGTCCTTCCTAAATGTC-3' R1 5'-CCTCAAACCCTCCCGTCTTC-3'	824 bp
F2 5'-ATGAGGCACCTGCTGATCAC-3' R2 5'-TAGTTGCGCTGGCCATAGTC-3'	927 bp
F3 5'-GCCCTACTACCGCCAGATTC-3' R3 5'-ACCATTCAGCCATTCCTCCG-3'	1355 bp

Supplemental Table 3. Microtubule sliding velocities and Student *t*-test values after the addition of purified PACRG or FAP20 protein to axonemes. The *p* values are a comparison to the same strain's control values.

Strain + µg PACRG	µm/sec +/- SEM	n	*p* value
wild-type control	17.10 +/- 0.43	114	
*pf18*control	14.00 +/- 0.55	52	
pf18 + 1 µg PACRG	15.01 +/- 0.55	43	*p*=0.20
pf18 + 2.5 µg PACRG	14.23 +/- 0.56	46	*p*=0.77
pf18 + 1 µg FAP20	13.97 +/- 0.50	49	*p*=0.96
pf18 + 2.5 µg FAP20	14.06 +/- 0.53	52	*p*=0.95
*pacrg (pf12)*control	13.93 +/- 0.43	58	
pacrg + 1 µg PACRG	14.73 +/- 0.49	49	*p*=0.29
pacrg + 2.5 µg PACRG	16.58 +/- 0.60	65	*p*<0.0001
*fap20 (*RL11) control	14.24 +/- 0.38	51	
fap20 + 1 µg FAP20	15.75 +/- 0.42	63	*p*=0.008
fap20 + 2.5 µg FAP20	16.86 +/- 0.42	52	*p*<0.0001

Supplemental Table 4. Antibodies and dilutions used for western analyses.

Antibody	kDa	Dilution	Source/Reference
PACRG	34	1:40,000	Ikeda et al, 2007
Rib72	72	1:10,000	Ikeda et al, 2003
FAP252	39	1:40,000	Ikeda/Kamiya Lab
Tektin	58	1:10,000	Yanagisawa and Kamiya, 2004
RSP1	123	1:40,000	Kohno et al, 2011
CaM-IP3	140	1:1000ap	Dymek and Smith, 2007
IC69	69	1:1000	King et al, 1985, Witman Lab
IC138	138	1:20,000	Hendrickson et al, 2004
DHC9	465	1:10,000	Yagi et al, 2009
DRC2/Ida6/FAP250	65	1:5,000	Bower et al, 2013
DRC1	79	1:5,000	Wirschell et al, 2013
Mia1/Mia2	76/35	1:10,000ea	Yamamoto et al, 2013
PF20	66	1:5,000	Smith and Lefebvre, 1997
Mbo2	110	1:5,000	Tam and Lefebvre, 2002
S-tag-protein-HRP		1:10,000	Millipore

References for Supplemental Table 4.

Bower, R., Tritschler, D., VanderWaal, K., Perrone, C.A., Mueller, J., Fox, L., Sale, W., and Porter, M.E. (2013) The N-DRC forms a conserved biochemical complex that maintains outer doublet alignment and limits microtubule sliding in motile axonemes. Mol Biol Cell, *24,* 1134-1152.

Dymek, E.E., and Smith, E.F. (2007). A conserved CaM- and radial spoke associated complex mediates regulation of flagellar dynein activity. J Cell Biol *179*, 515-526.

Hendrickson, T.W., C.A. Perrone, P. Griffin, K. Wuichet, J. Mueller, P. Yang, M.E.Porter, and W.S. Sale. 2004. IC138 is a WD-repeat dynein intermediate chain required for light chain assembly and regulation of flagellar bending. *Mol. Biol. Cell*. 15:5431–5442.

Ikeda, K., Brown, J.A., Yagi, T., Norrander, J.M., Hirono, M., Eccleston, E., Kamiya, R., and Linck, R.W. (2003). Rib72, a conserved protein associated with the ribbon compartment of flagellar microtubules and potentially involved in the linkage between outer doublet microtubules. J Biol Chem *278*, 7725-7734.

Ikeda K., Ikeda T., Morikawa K., and Kamiya R. (2007). Axonemal localization of *Chlamydomonas* PACRG, a homologue of the human Parkin-coregulated gene product. Cell Motil Cytoskeleton *64*, 814–821.

Kohno, T., Wakabayashi, K., Diener, D.R., Rosenbaum, J.L., and Kamiya, R. (2011) Subunit interactions within the *Chlamydomonas* flagellar spokehead. Cytoskeleton 68, 237-246.

Smith, E. F., and P. A. Lefebvre.1997. The role of central apparatus components in flagellar motility and microtubule assembly. CellMotil. Cytoskeleton *38,* 1–8.

Tam, L.W. and Lefebvre, P.A. (2002). The *Chlamydomonas MBO2* locus encodes a conserved coiled-coil protein important for flagellar waveform conversion. Cell Motil Cytoskeleton*51*, 197-212.

Wirschell, M., Olbrich, H., Werner, C., Tritschler, D., Bower, R., Sale, W.S., Loges, N.T., Pennekamp, P., Lindberg, S., Stenram, U., Carlen, B., Horak, E., Kohler, G., Nurnberg, P., Nurnberg, G., Porter, M.E., and Omran, H. (2013). The nexin link-DRC subunit DRC1/CCDC164 is essential for motile cilia function in algae and humans. Nature Genet., *published online January 27, 2013*

Yagi, T., Uematsu, K., Liu, Z., and Kamiya, R. (2009). Identification of dyneins that localize exclusively to the proximal portion of *Chlamydomonas* flagella. J Cell Sci *122*, 1306-1314.

Yamamoto, R., Song, K., Yanagisawa, H., Fox, L., Yagi, T., Wirschell, M., Hirona, M., Kamiya, R., Nicastro, D., and Sale, W.S. 2013. The MIA complex is a conserved and novel dynein regulator essential for normal ciliary motility. J Cell Biol *201,* 263-278.

Yanagisawa, H.A., and Kamiya, R. (2004). A tektin homologue is decreased in *Chlamydomonas* mutants lacking an axonemal inner-arm dynein. Mol Biol Cell *15*, 2105-2115.

Supplemental Table 5. The *C. reinhardtii* strains used in cryo-ET analysis.

Strains	Number of tomograms	Averaged repeats	Resolution (nm)
wild-type (CC4533*)	19	2381	2.3
pacrg(CLiP 159)	19	2333	2.7
pacrg; fap20	13	1826	2.4

*the background strain used in the *Chlamydomonas* Library Project (www.chlamylibrary.org), with normal motility and axonemal structures.